



**Influence of Charge Sequence on the Adsorption of
Polyelectrolytes to Oppositely-Charged Polyelectrolyte
Brushes**

Journal:	<i>Soft Matter</i>
Manuscript ID	SM-ART-03-2019-000581.R1
Article Type:	Paper
Date Submitted by the Author:	30-May-2019
Complete List of Authors:	Sethuraman, Vaidyanathan; University of Minnesota Twin Cities, Chemical Engineering and Materials Science McGovern, Michael; University of Minnesota Twin Cities, Chemical Engineering and Materials Science Morse, David; University of Minnesota Twin Cities, Chemical Engineering and Materials Science Dorfman, Kevin; University of Minnesota Twin Cities, Chemical Engineering and Materials Science

Cite this: DOI: 00.0000/xxxxxxxxxx

Influence of Charge Sequence on the Adsorption of Polyelectrolytes to Oppositely-Charged Polyelectrolyte Brushes[†]

Vaidyanathan Sethuraman,^{a‡} Michael McGovern,^{a‡} David C. Morse,^{a*} and Kevin D. Dorfman^a

Received Date

Accepted Date

DOI: 00.0000/xxxxxxxxxx

When a solution of polyanionic chains is placed in contact with a polycationic brush, the polyanions adsorb into the brush. We investigate the influence of the charge sequences of the free and bound species on the thermodynamics of polyelectrolyte adsorption. As model systems, we consider free and brush polyelectrolytes with either block or alternating charge sequences, and study the adsorption process using coarse-grained Langevin dynamics with implicit solvent, explicit counterions, and excess salt. Free energy, internal energy, and entropy of adsorption are computed using umbrella sampling methods. When number of polyanions exceed the number of polycations, the brush becomes overcharged. Free chains adsorb most strongly when both free and tethered chains have a block charge sequence, and most weakly when both species have an alternating sequence. Adsorption is stronger when the free polyanion has a block sequence and the tethered polycation is alternating than in the reverse case of an alternating free polymer and a tethered block copolymer. Sequence-dependent effects are shown to be largely energetic, rather than entropic, in origin.

1 Introduction

Complex coacervation is a liquid–liquid phase separation phenomenon wherein oppositely charged polyelectrolytes phase separate into a polyelectrolyte-rich phase (coacervate) and a polyelectrolyte–dilute phase (supernatant) when they are mixed together in solution. Complexes formed by these oppositely charged polyelectrolytes play a crucial role in many technologically and biologically important processes.^{1–10} For instance, complex coacervates involving proteins play important roles in targeted drug delivery.^{11–14} Polyelectrolyte multilayers are another important application involving complexation between oppositely charged polyelectrolytes.^{15–18} The adsorption of alternating layers is believed to be driven by overcompensation of charge when a new layer of polyelectrolyte is added, which leaves a net charge that attracts the next layer of oppositely charged polyelectrolyte.¹⁹ Simulations in such contexts have looked at the effects of chain length and sequence on the morphology of the films that are formed.²⁰ Recently, there has been increased interest in understanding the role of charge sequence on the formation of polyelectrolyte complexes, focusing largely on the complexation

of these polyelectrolytes in solution.^{21,22} In the present contribution, we bring together these two research themes, employing coarse-grained molecular dynamics simulations of a polyelectrolyte brush system to investigate how charge sequence affects adsorption of polyanions and eventual overcharging of a polycationic brush in the presence of a solution of polyanions and excess salt.

The starting point for understanding the complexation of oppositely charged polyelectrolytes is the Voorn–Overbeek (VO) model,²³ which combines a Flory–Huggins expression for the entropy of mixing with a Debye–Hückel level description of electrostatics to compute the free energy of the solution. Despite its simplicity, the VO model captures the main qualitative features of the phase diagram. Phase separation is driven by favorable electrostatic interactions in the more concentrated phase, and by the entropy gained by release of counterions, which exceeds the loss of entropy arising from partitioning of polymers into the coacervate. While the VO model is a useful starting point, it is based on a highly simplified description of electrostatic correlations that neglects the effects of polymer connectivity and underestimates the importance of correlations in the dilute phase. As a result, the VO model has been extended in various ways to take into account these additional effects.^{24–32}

Early observations of some polyelectrolyte systems showed that the assumption of an uncorrelated dilute phase was rather a poor one. For instance, models were proposed to account for pairing of oppositely charged polyelectrolytes in solution below their critical concentration for phase separation and at low salt concentrations.^{28,33} Other models introduced correlations be-

^{a*} Department of Chemical Engineering and Materials Science, University of Minnesota –Twin Cities, 421 Washington Ave. SE, Minneapolis, MN 55455, USA. E-mail: morse012@umn.edu

^a Department of Chemical Engineering and Materials Science, University of Minnesota –Twin Cities, 421 Washington Ave. SE, Minneapolis, MN 55455, USA. E-mail: dorfman@umn.edu

[†] Electronic Supplementary Information (ESI) available: See DOI: 00.0000/00000000.

[‡] Additional These authors contributed equally to this work.

tween polyelectrolytes and their counterions to capture the entropic effects of counterion release.^{26,30,34} Models based on self-consistent field theory were also introduced to describe the effects of charge connectivity to varying levels of approximation.^{24,35–40} Recent works by Sing and coworkers have explored the effects of polymer stiffness, and salt valency on a variety of polyelectrolyte charge sequence architectures in bulk.^{21,41,42} Their results showed that the thermodynamics of coacervation is strongly correlated to the entropic confinement of condensed counterions along the polymer backbone, which in turn is dependent on the backbone charge sequence.²¹

Several other groups have also performed simulations on other closely related systems such as adsorption of charged proteins onto polyelectrolyte brushes.^{13,35,43–46} Strong adsorption of the charged proteins to the polyelectrolyte brush is found even when both the brush and protein have the same net charge⁴⁷ or when two polyelectrolytes possessing the same charge mix in bulk.⁴⁸ When the charge ratio of the polyelectrolytes in solution differs from unity, a net charge may be present on the complexes, which is often referred to as “overcharging” of the complex. Shklovskii and co-workers proposed a model for this phenomenon where overcharging of complexes is primarily driven by the elimination of the free chain electrostatic self-repulsion energy upon complexation. The excess charge tends to be spread out over the whole complex in the condensed phase, lowering the electrostatic energy.^{49–51} While the complex formation at a charge ratio of unity is driven by counterion release – an entropic effect, the overcharging of the complexes is driven by change in electrostatic correlation energy upon adsorption.

In the present contribution, we consider how charge sequence affects the adsorption of polyanions into a polycation brush, with an emphasis on the overcharging of the brush. Specifically, we explore how different charge sequences in the tethered (brush) and untethered (free) polyelectrolytes affect the strength of adsorption and the distribution of charges within the brush. To answer these questions, we consider two different types of charge sequences: (i) diblock copolymers, in which the charged groups are all contained within a single block of the polyelectrolyte; and (ii) alternating copolymers, for which charged and uncharged groups alternate along the backbone. We employ coarse-grained Langevin dynamics simulations of a polyelectrolyte model in the presence of excess salt to compute both the composition and charge of the brush as a function of the total amount of free polyanion in the system for all four possible combinations of isomers. Since one polyelectrolyte species (the polycation) is constrained to be within the brush, there is an asymmetry between the two types of polyelectrolyte, apart from any difference arising from different charge sequences. The system we examine here is distinct from prior work on layer-by-layer deposition, in which both polyelectrolyte species have generally been taken to have the same type of charge sequence.^{20,45} In order to understand more deeply the thermodynamics of the adsorption process, we use umbrella sampling simulations to calculate the free energy of adsorption, and simulations with an added step potential to calculate the change in internal energy due of adsorption of polyelectrolytes. We thus elucidate the relative importance of changes

of entropy and internal energy upon adsorption, which have not been measured in previous simulation works.

2 Methodology

2.1 Description of the System Setup and Systems Studied

Figure 1(a) provides a schematic representation of the bead-spring polyelectrolyte model used in this work. Each free polyanion consists of 15 negatively charged beads and 15 neutral beads. For an alternating polyanion, the charged and neutral beads alternate along the chain. For a block polyanion, the beads are arranged into a single charged block and a single neutral block. In order to minimize the effect of the wall, each tethered polycation is a chain of 40 beads that contains a spacer block of 10 neutral beads (with the terminal bead tethered to the surface) followed by a section containing 15 charged and 15 neutral beads that may either alternate or be arranged in blocks. A tethered block polycation thus consists of a tethered block of 25 neutral beads (including the spacer block) connected to a block of 15 charged beads, with the charged block at the free end of the polymer. A tethered alternating polycation instead consists of a spacer block of 10 neutral beads attached to a segment of 30 alternating charged and neutral beads, in which the bead at the free end is charged. The neutral bead in contact with the wall is free to move in the x and y direction, but is constrained to the wall by setting the z -component of the force and velocity to zero and constraining the z -coordinate. Although grafted monomers are allowed to traverse in the $x-y$ plane, they do not show any tendency to clump under the conditions used here (see Fig. S1 of the Supplemental Material).

Inasmuch as the wall is not charged, the problem formulation does not depend on the choice of whether the tethered chains are polycations and the free chains are polyanions, or the reverse. Without loss of generality, we chose the “free” chains to be polyanions and the tethered chains to be polycations. Note that the polyanions are all “free” only in the sense that they are not tethered to the wall, though some or all of these chains may be physically adsorbed to the brush. For each charged polyelectrolyte bead in this system, there is an oppositely charged counterion bead, in addition to excess salt ions. Figure 1(b) provides a snapshot of the resulting system after equilibration. All beads have the same size σ and mass m , but the size of free ion beads have been reduced in Figure 1(b) to clearly depict the polyelectrolyte chains.

Figure 1(c) displays a schematic illustration along with the corresponding nomenclature for the four different configurations employed in this study. For instance, the top right panel of Figure 1(c) depicts a case wherein the polycation brush possesses a block architecture whereas the free polyanion possesses an alternating architecture. The nomenclature for such a configuration is then Block-Alter, where the former part of the nomenclature corresponds to the charge sequence in the polycation brush and the latter part corresponds to the charge sequence in the free polyanions. The description of a tethered polycation as “alternating” refers only to the arrangement of the last 30 beads, since all tethered chains contain a spacer block of 10 neutral beads with the

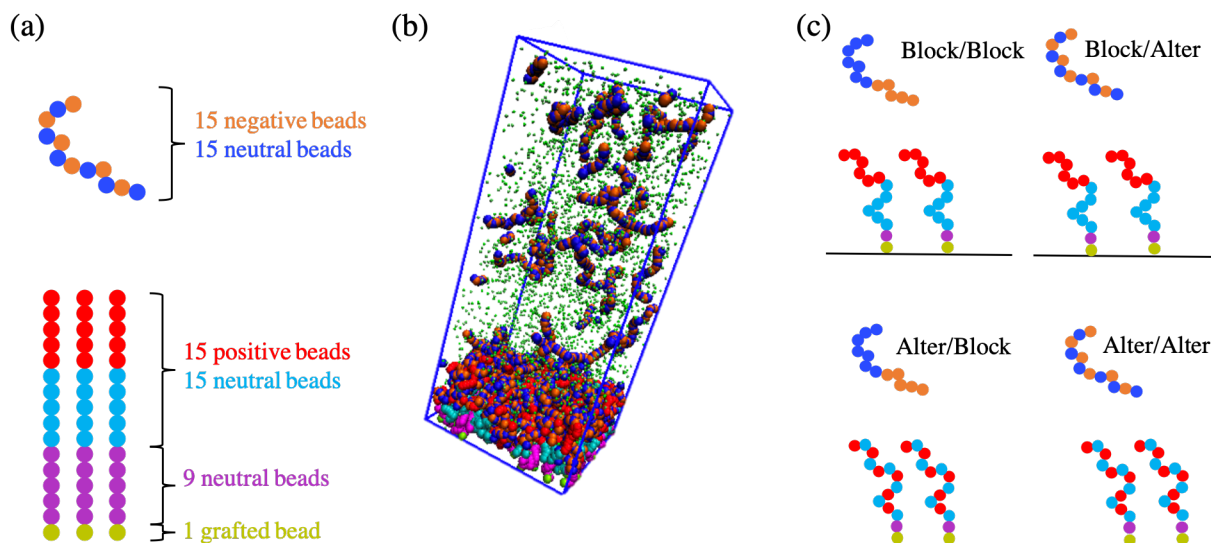


Fig. 1 (a) Schematic illustration of the polycationic brush and polyanions in solution. All the polyanions consist of 15 negatively charged beads (red) and 15 neutral beads (cyan), with this particular “free” macromolecule being an alternating polyanion. The polycations contain a spacer block (shown in magenta) with one end connected to a grafted monomer (dark yellow). Other end of the spacer block is connected to a terminal segment which comprises 15 positively charged beads (orange) and 15 neutral beads (blue), with this particular brush being formed by block polycations; (b) Snapshot of the simulation box. Color coding identical to part (a) is utilized here as well. The ions, both excess salt and the polyelectrolyte’s counterions, are reduced in size for clarity. Snapshots are obtained using Visual Molecular Dynamics (VMD) software;⁵² (c) Schematic illustration of the four configurations utilized in this study. The corresponding nomenclature for each configuration is also given in the schematic. The solid line depicts the grafted surface. In (a) and (c) the number of beads shown in the schematics do not correspond to the actual number of beads employed in our simulations.

first bead connected to the wall.

2.2 Simulation Technique

To avoid bead–bead overlap, all non–bonded particles in the system interact through a repulsive Weeks-Chandler-Anderson (WCA) potential (U_{WCA}),

$$U_{\text{WCA}} = \begin{cases} 4\epsilon_{\text{WCA}} \left[\left(\frac{\sigma}{r}\right)^{12} - \left(\frac{\sigma}{r}\right)^6 + \frac{1}{4} \right] & r \leq 2^{\frac{1}{6}}\sigma \\ 0 & r > 2^{\frac{1}{6}}\sigma \end{cases} \quad (1)$$

where ϵ_{WCA} and σ represent the interaction parameter between the particles and the diameter of the particles, respectively. We use energy and length units in which $\epsilon_{\text{WCA}} = 1.0$, and $\sigma = 1.0$. All simulations are performed at a reduced temperature⁵³ $T = 1$.

Bonded beads within each polymer interact through a FENE bonded potential with a non-zero rest length,

$$U_{\text{FENE}} = 4\epsilon_{\text{FENE}} \left[\left(\frac{\sigma}{r}\right)^{12} - \left(\frac{\sigma}{r}\right)^6 + \frac{1}{4} \right] - \frac{KR_0^2}{2\sigma^2} \ln \left[1 - \left(\frac{r}{R_0}\right)^2 \right], \quad (2)$$

with $K = 30$, $R_0 = 1.6\sigma$, and $\epsilon_{\text{FENE}} = 1.5$. The first term of the bonded potential accounts in Eq. 2 accounts for the non–bonded interactions between bonded monomers. To avoid double counting, the non–bonded potential (Eq. 1) is excluded for these 1–2 interactions. Further, a harmonic cosine angle potential (U_θ), in addition to the non–bonded potential, is applied to all polymer

beads separated by two bonds,

$$U_\theta = \kappa(1 + \cos\theta), \quad (3)$$

with $\kappa = 3$.

The system is periodic in the x and y dimensions, but finite in the (vertical) z –dimension, with a simulation box size of $53\sigma \times 53\sigma \times 120\sigma$. The particles are constrained to remain within the box by repulsive wall potentials that diverge at $z = 0$ and $z = L_z = 120.0\sigma$,

$$U_{\text{wall}} = \begin{cases} 4\epsilon_w \left[\left(\frac{\sigma}{2z}\right)^{12} - \left(\frac{\sigma}{2z}\right)^6 + \frac{1}{4} \right] & z \leq 2^{\frac{1}{6}}\sigma \\ 0 & z > 2^{\frac{1}{6}}\sigma \end{cases} \quad (4)$$

with $\epsilon_w = 0.5$. The terminal bead of the spacer block of each tethered chain is constrained to lie in the plane $z = 0.5\sigma$.

All the charged monomers and the free ions are assigned charges of ± 1 . The dielectric constant of the implicit solvent is chosen so as to give a Bjerrum length equal to σ , the range of the pair interaction. The particle-particle-particle mesh (P3M) method is used to compute electrostatic interactions^{54,55}, with parameters chosen to give a maximum relative error of 10^{-5} in forces. A slab geometry⁵⁶ is used to account for non-periodicity in the z –dimension, in which the periodic unit cell used in the computation of electrostatic forces is taken to be 3 times longer in the z direction that the length of the region to which the particles are confined.

The simulation system contains 64 tethered polycation chains

($N_{pc} = 64$) for all cases considered in this work. We have simulated cases in which the number of free polyanion chains N_{pa} is 16, 32, 48, 64, 80, and 100. For each charged bead of the polymer, there exists a counter-ion of the opposite charge. All our simulation systems thus correspond to a dissociated polyelectrolyte with fixed salt concentration. All simulations reported here contain 1020 excess salt ions (510 of each sign) in addition to the counterions required to neutralize the polyelectrolyte charges. For each value of N_{pa} , we obtained data for all 4 possible combinations of block and alternating architectures, *i.e.*, block–block, block–alternating, alternating–block and alternating–alternating, where the first part of the notation refers to the polycation brush and the latter part refers to the polyanions in solution. Simulations are performed using the LAMMPS⁵⁷ package for at least 1.8×10^7 time steps using a time step between 0.005 – 0.01 in Lennard-Jones units and the equations of motion are evolved using a Langevin dynamics integrator with a damping factor of 7.0 (typical values lie between 1 and 10) in reduced units.⁵³

The extent of overlap between neighboring tethered polymers can be estimated by comparing the average area per tethered molecule Σ to the square of the height h of the tethered layer. The maximum brush extension is chosen to be the z coordinate value where the brush density decays to 95 % of its maximum value. For the simulations presented here, $\Sigma \simeq 44\sigma^2$, while $h \simeq (22 - 27)\sigma$, giving $h^2/\Sigma \simeq 10$. In these simulations, the tethered layer is thus a rather weakly overlapping polymer brush.

2.3 Quantification Measures

2.3.1 Number of Adsorbed Polyanions

To quantify adsorption, we need the average number of polyanion chains that are adsorbed into the brush of tethered polycations. For this purpose, we consider a polyanion chain to be adsorbed if at least one of its monomers (charged or neutral) is within a prescribed cut-off distance (r_c) of any polycation brush monomer, excluding the neutral beads connecting the charged monomers to the grafted surface. In the context of atomistic simulations, the cut-off distance is conventionally chosen as the position of the first minimum of the radial distribution function of the entities of interest. However, owing to the level of coarse-graining in our simulations, we do not see any distinct minimum in the polyanion-polycation radial distribution function (see Fig. S2). Hence, we choose a cut-off $r_c = 1.50 \sigma$ slightly larger than the range of the pair interaction. The number of adsorbed chains is found to be relatively insensitive to the choice of cut-off for all distances $r_c \leq 2.0 \sigma$.

2.3.2 Energy of Adsorption

The energy of adsorption was measured by performing simulations in which a repulsive bias potential is used to exclude 5 labeled polyanions from the polymer brush, and computing the difference between the average energy obtained from biased and unbiased simulations (no external bias potential) of otherwise identical systems. In these biased simulations, an additional repulsive

potential of the form

$$U_{\text{bias}} = \begin{cases} k_{\text{bias}} (z_{\text{brush}} - z) & z \leq z_{\text{brush}}, \\ 0 & z > z_{\text{brush}}, \end{cases} \quad (5)$$

is applied to each monomer in each of the five particular polyanions. Here k_{bias} and z_{brush} are parameters, for which we choose $k_{\text{bias}} = 1 k_{\text{B}}T/\sigma$ and $z_{\text{brush}} = 40 \sigma$. This value for z_{brush} is chosen to be significantly greater than the average brush height of approximately 15σ in order to guarantee that excluded chains do not interact with any tethered chains. These biased simulations were performed for polyanion concentrations $N_{pa} \in \{32, 48, 64, 72\}$, and for each of the four isomer combinations.

The difference between the average energy of the biased and the unbiased simulations is denoted by ΔU_{tot} . The corresponding difference in the average number of adsorbed polymers is denoted by ΔN . Results for these quantities are displayed in Fig. S3(a) of the supplemental material. The incremental change in internal energy per additional adsorbed polymer, denoted by ΔU , is computed by evaluating the ratio $\Delta U_{\text{tot}}/\Delta N$.

Figure S3(b) displays the difference ΔN in the average number of adsorbed chains between the biased and unbiased simulations. When the number of graft chains, N_{pc} , is greater than the number of free chains, N_{pa} , almost all chains are adsorbed except those which are prevented from doing so by the bias potential. In these cases, ΔN is almost exactly equal to the number of polyanion chains that are excluded from the brush by the bias potential. When $N_{pa}/N_{pc} > 1$, however, the difference ΔN is controlled by the change in the chemical potential of the unlabeled polyanions that is caused by the exclusion of the five labeled polyanions from the brush. This results in a difference ΔN that becomes very small when the number of remaining unlabeled free polyanions substantially exceeds the number of tethered polymers, both because the extent of adsorption becomes a slowly varying function of free copolymer concentration in this region, and because the number of labeled chains excluded from the brush eventually becomes a small fraction of the average number of free polymers. For the same reason, ΔU_{tot} also becomes very small in this limit. This leads to a very large numerical uncertainty in our results for ΔU at large values of N_{pa}/N_{pc} . As a result, we are able to obtain statistically meaningful results for ΔU only over a very limited range when N_{pa}/N_{pc} is greater than unity.

2.3.3 Free Energy and Entropy of Adsorption

Umbrella sampling simulations have been performed to compute the free energy $F_c(z)$ of a molecule whose center-of-mass is constrained to lie a distance z from the wall.^{58,59} In these simulations, a harmonic bias is applied to the z -coordinate of the center of mass of one randomly chosen polyanion. Positions of the minima of these harmonic potentials were chosen to ensure overlap between the distribution of center of mass positions (see Fig. S4(c) of the supplemental material). Simulations were performed using constraining potentials within minima at $z = 5, 8, 10, 12, 14, 16, 18, 22, 26, 30, 32, 34, 38, 42, 46, 50$, and 54 using a force constant value of $0.4 k_{\text{B}}T/\sigma^2$. Examples of the resulting constrained free energy $F_c(z)$ for $N_{pa} = 32$ and $N_{pa} = 80$

are shown as a function of z in Figs. S4(a) and S4(b) respectively. To generate the initial configurations of umbrella sampling, a steered molecular dynamics simulation⁶⁰ is performed by pulling one chain with a constant force. The resulting free energy from the umbrella sampling simulations is calculated using the Weighted Histogram Analysis Method (WHAM)⁶¹ using the open-source code provided by the Grossfield lab.⁶² Further details on the parameters utilized for simulations are given in Sec. S5 of the Supplementary Material. All bias calculations are performed using the COLVARS module⁶³ within the LAMMPS package.

The average free energy of adsorption, denoted by ΔF , is defined by a Boltzmann-weighted average

$$\Delta F = \frac{\int_0^{L_0} \Delta F_c(z) \exp(-\beta \Delta F_c(z)) dz}{\int_0^{L_0} \exp(-\beta \Delta F_c(z)) dz}, \quad (6)$$

where $\beta = 1/k_B T$, and $\Delta F_c(z)$ is defined as the difference between the constrained free energy $F_c(z)$ for a given z and that in the bulk, and L_0 is a cutoff length.

The dominant contribution to either the numerator or denominator ΔF in Eq. 6 arises from the region near the minimum of $\Delta F_c(z)$. The integrand within the numerator of Eq. 6 decays rapidly to zero within a few σ . As a result, ΔF is insensitive to the exact value chosen for L_0 . We have chosen L_0 to be the sum of the maximum brush extension (h_b) and five times the Debye length (λ_D).

The Debye length λ_D in reduced units is calculated using

$$\lambda_D = \left(\frac{4\pi e^2}{\epsilon_r k_B T} \sum_j n_j z_j^2 \right)^{-1/2}. \quad (7)$$

Here, ϵ_r is reduced dielectric constant, e is the elementary charge, j is an index for species of free ions (counterions and excess salt), n_j and z_j are the concentration and valence (± 1) of species j , respectively, and the sum is taken over species of free ions. For the parameters chosen in this study, Debye length for a polymer free system ($N_{pa} = N_{pc} = 0$) is $\simeq 5.1\sigma$ and that when the number of polyanions and polycations ($N_{pa}/N_{pc} = 1$) is $\simeq 3.0\sigma$. Figures S5(a) and S5(b) display the maximum brush extension and the Debye length respectively, for all the cases studied.

To compare with experiments, we note that the ratio between the steric diameter σ , to the Debye length λ_D is approximately 0.3. Our simulations thus correspond to an experimental system with 0.3 - 0.7 M sodium chloride solution in water (average steric diameter of 0.588 nm and an experimentally measured Debye length of approximately 0.5 nm)⁶⁴.

The entropy of binding per chain, denoted by ΔS , is given by the difference

$$-\Delta S = (\Delta F - \Delta U)/T. \quad (8)$$

Here, ΔF is the average binding free energy defined in Eq. 6 and ΔU is the change in internal energy per chain due to adsorption. Values for ΔS were obtained only for those values of N_{pa} at which we were able to compute accurate values of ΔU .

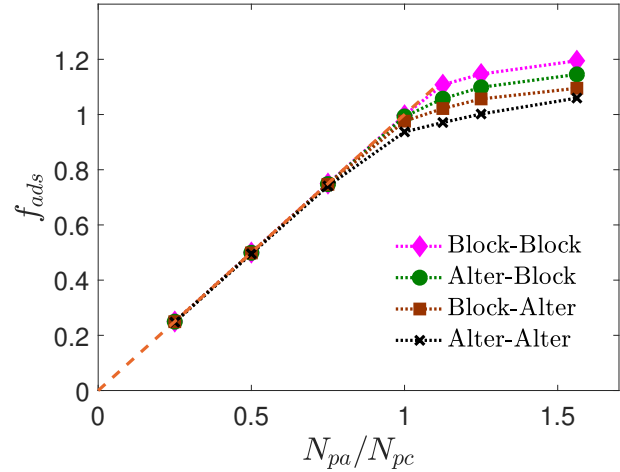


Fig. 2 Ratio ($f_{ads} = N_{pa,adsorbed}/N_{pc}$) of the number of polyanion chains bound to the polyelectrolyte brush to the total number of polycation chains in the system as a function of the ratio (N_{pa}/N_{pc}) of the total number of polyanion to polycation chains. The orange dotted line corresponds to the linear relationship $f_{ads} = N_{pa}/N_{pc}$, that is obtained if all the polyanions are adsorbed. Error bars are smaller than the symbol size.

2.3.4 Charge within the Brush Region

We compute the charge density $q(z)$ as a function of distance from the grafted surface using

$$q(z) = \sum_{j=0}^{I_t} n_{t,j}(z) q_j, \quad (9)$$

where I_t , $n_{t,j}(z)$, and q_j represent the total number of species (ions and polymers), number concentration of monomers of each species at a distance z from the grafted surface, and the charge per monomer on the corresponding species respectively. Corresponding concentrations of all polycation and polyanion monomers (charged and neutral) are denoted by $\rho_{pc}(z)$ and ρ_{pa} , respectively. To compute the overall bound charge Q_b within the brush, initially we define the “brush region” as the region bounded between the grafted surface and the plane where the concentration of the polycations ρ_{pc} within the brush falls to 5% of its maximum value. The net charge within the brush region is then calculated using

$$Q_b = \int_0^{z_c} q(z) dz, \quad (10)$$

where z_c denotes the z coordinate of the plane wherein ρ_{pc} falls to 5% of its maximum value.

3 Results and Discussion

3.1 Ratio of Adsorbed to Tethered Polyanions

We begin our discussion of the influence of charge sequence by considering the extent of adsorption. Let f_{ads} denote the ratio of the number of adsorbed polyanion chains to the total number of tethered polycation chains. In what follows, we will refer to a brush as “undercharged” when $f_{ads} < 1$ and “overcharged” when $f_{ads} > 1$. By this definition, a brush is said to be overcharged if the charge associated with adsorbed polyanions is greater than

that required to compensate the charge of the tethered polycations, and "undercharged" if the charge of the polycations is instead compensated in part by an excess of small anions in and near the brush.

Figure 2 displays f_{ads} plotted versus the ratio N_{pa}/N_{pc} of the total number of polyanions in the system (adsorbed and free) to the total number of tethered polycations. In this plot, a line $f_{ads} = N_{pa}/N_{pc}$ of slope 1 (shown by the dashed orange line) corresponds to a situation in which all of the polyanions are adsorbed. A value of $f_{ads} = 1.0$ corresponds to a situation in which the number of adsorbed polyanions exactly matches the number of tethered polycations. Error bars show standard deviation due to statistical errors⁶⁵ computed by a methodology described in Sec. S7 of the supplemental material.

In systems with $N_{pa}/N_{pc} \leq 1$, we find that essentially all of the polyanion chains in our simulation are adsorbed, as indicated by collapse onto the line $f_{ads} = N_{pa}/N_{pc}$. This strong binding to an undercharged brush is primarily driven by the gain in entropy arising from counterion release, as discussed in Sec. 3.2.

In systems with $N_{pa}/N_{pc} > 1$, the fraction f_{ads} slightly exceeds 1, indicating slight overcharging, but f_{ads} remains less than N_{pa}/N_{pc} , indicating that some excess polyanions remain free. In this regime, f_{ads} increases slowly with increasing number of polyanions. Most polyanions added in excess of the number required to neutralize the brush thus remain free. Notably, the degree of overcharging in this regime, as quantified by the difference $f_{ads} - 1$, depends on chain architecture. The strongest adsorption occurs when both the polycations and polyanions have a block architecture. The weakest adsorption occurs when both types of chain possess an alternating architecture. The two cases in which one type of chain has a block architecture and the other is alternating fall between these extremes. Slightly stronger adsorption is obtained in the the Alter-Block case of an alternating tethered polycation and a block polyanion then for the Block-Alter case of a block polycation and an alternating polyanion.

3.2 Thermodynamics of Adsorption

To clarify the thermodynamic origins of the observed behavior, we consider the behavior of the free energy of adsorption ΔF (Eq. 6), and the energy and entropy change upon adsorption, denoted by ΔU and ΔS respectively. Figure 3 displays the adsorption free energy ΔF as a function N_{pa}/N_{pc} for all four combinations of charge sequence. For the two cases with $N_{pa}/N_{pc} < 1$, ΔF is strongly negative (at least $10 k_B T$) for all four cases, implying strong binding. Since the probability of adsorption depends exponentially on ΔF , this is consistent with the conclusion that nearly all polyanions are adsorbed in this regime, as shown in Fig. 2. By measuring ΔF , we can see, however, that while binding is strong for all charge sequences for $N_{pa}/N_{pc} \leq 1$, the binding free energy is largest for the Block-Block charge sequence and smallest for the Alter-Alter charge sequence, with the other two cases intermediate between these extremes. In systems with $N_{pa}/N_{pc} \leq 1$, the Block-Block case is significantly more strongly bound than the other three cases. In systems with $N_{pa}/N_{pc} > 1$, the binding energies for all four sequences are weaker ($3 - 6 k_B T$), but the order of different se-

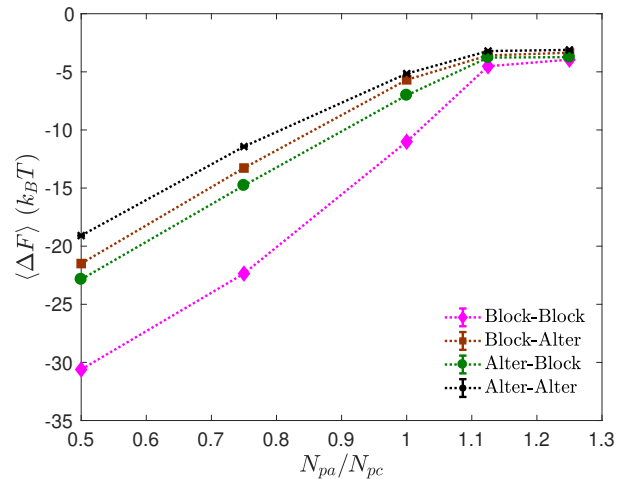


Fig. 3 Adsorption free energy ΔF as a function of the ratio between the number of polyanions to polycations in the system N_{pa}/N_{pc} . Error bars are smaller than the symbol size.

quences is the same for systems with $N_{pa}/N_{pc} \leq 1$, consistent with our observations regarding the sequence dependence of the magnitude of f_{ads} .

We compute the energetic and enthalpic penalties to the free energy to determine (i) the origins in the differences in the free energy for different charge sequence; and (ii) whether adsorption is energetically or entropically driven. Figure 4 shows the energy change ΔU associated with adsorption and the corresponding gain in entropic free energy $T\Delta S = \Delta U - \Delta F$, both of which are plotted versus N_{pa}/N_{pc} . Several trends become clear upon inspection of these graphs.

Focusing first on the sequence dependence of the energy and entropy, we note that the dependence of the entropic contribution $T\Delta S$ on N_{pa}/N_{pc} is almost the same for all four cases, whereas the magnitude of the energy of adsorption is significantly different for different combinations of charge sequences. The differences between the free energies of adsorption for different cases thus arise primarily from difference in the adsorption energy ΔU . Values of ΔU in each case depend rather weakly on N_{pa}/N_{pc} , but differ significantly with respect to charge sequence. The ordering of the magnitudes of binding energy for different cases is consistent with the ordering observed for the total free energy. The largest binding energy is obtained for the Block-Block case and the smallest for the Alter-Alter case. The differences in adsorption free energy and resulting strength of adsorption in different cases thus seem to arise primarily from differences in electrostatic binding energy, rather than from differences in entropy.

We focus next on the relative magnitude of the entropic and energetic contributions to the overall binding free energy. Note that the entropic contribution to the free energy of binding generally dominates in the case of strongly undercharged brushes, with many more tethered chains than adsorbed chains. At the lowest value of $N_{pa}/N_{pc} = 0.5$ studied here, the two contributions are comparable only for the Block-Block case, for which $\Delta U \simeq -15 k_B T$ and $T\Delta S \simeq 16 k_B T$. The entropic contribution decreases

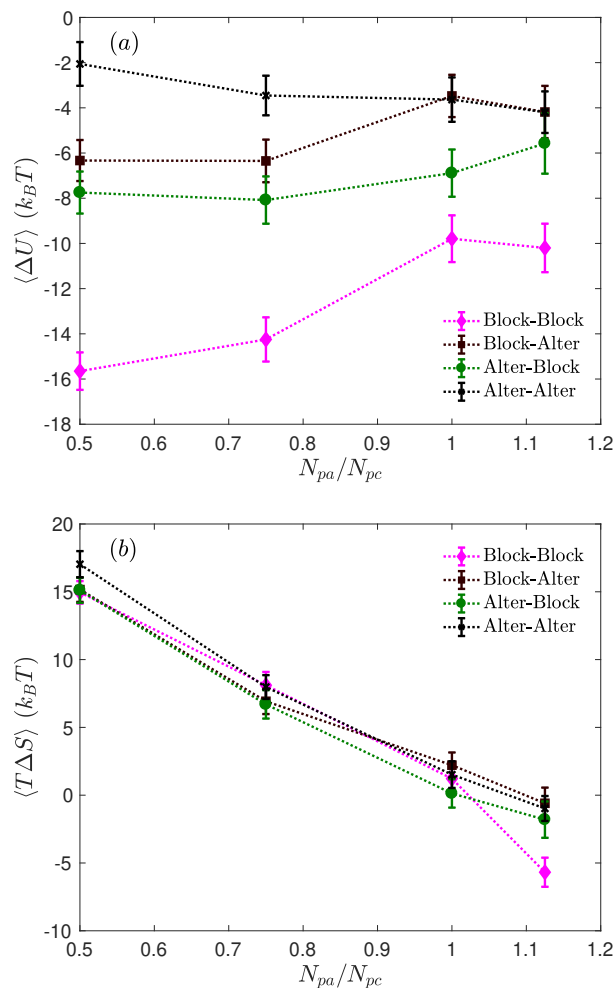


Fig. 4 (a) Internal energy of adsorption per chain; (b) Entropy difference per chain between biased and unbiased systems.

steadily with increasing values of the ratio N_{pa}/N_{pc} , however, and nearly vanishes for $N_{pa}/N_{pc} = 1$. Adsorption is thus driven primarily by entropy gain for strongly undercharged systems whereas energy decrease is important in nearly neutral and overcharged systems. Although a direct parallel cannot be drawn, it is interesting to note that the recent study by Rathee *et al.*²² showed that the association of equal number of oppositely charged polyelectrolytes in the bulk Bjerrum length of 1σ is *energetically* driven when the polymers do not dissociate, which are seemingly at odds with our study.

We assume that the large value of ΔS in systems with $f_{ads} \ll 1$ reflects the entropy gain arising from the release of counterions when a polyanion is added to the brush. This increase in entropy is primarily a result of the transfer of counterions from a region within the brush with a relatively high concentration of counterions to a bulk solution with a much lower counterion concentration. As f_{ads} increases, however, the concentration of counterions remaining within the brush decreases, as small anions are replaced by polyanions, and the entropy gain per added polyanion steadily decreases. Consider a simple picture of this process in which we assume that $f_{ads} = N_{pa}/N_{pc}$ for all $N_{pa}/N_{pc} \leq 1$. This pic-

tures suggests that, as N_{pa}/N_{pc} approaches unity from below, the charge of the tethered polycations becomes almost entirely compensated by the charge of the adsorbed polyanions. In this limit, the concentration of small counter-anions within the brush should become almost equal to that outside the brush, causing the entropy gain arising from counterion release to vanish. This simple picture is at least roughly consistent with our results, which yield a very small value of $T\Delta S$ for $N_{pa}/N_{pc} = 1$, for which $f_{ads} \simeq 1$.

Results for ΔU and $T\Delta S$ can be obtained only for a narrow range of values of $N_{pa}/N_{pc} > 1$. This is a result of limits on the statistical accuracy with which we can determine ΔU in this regime. Over the range in which we can obtain reliable values, however, it appears that ΔF is dominated in this regime by the energy change ΔU . The energetic contribution is particularly large in this regime in Block-Block and Alter-Block cases wherein the untethered polyanion is a diblock copolymer. Note that, for overcharged systems, the adsorption energy seems to depend more strongly upon the charge sequence of the free polyanion than on the sequence of the tethered polycation, since very similar values of ΔU are obtained for the Alter-Alter (black) and Block-Alter (brown) cases for which the free polyanions are alternating, with a somewhat larger value for the Alter-Block (green) case. Local correlations within a brush containing tethered alternating polycations and adsorbed block polyanions are presumably rather similar to those within a brush containing tethered block polycations and alternating free polyanions. The greater sensitivity of ΔU to the sequence of the free polymer may thus reflect differences between the electrostatic energies of free (non-adsorbed) alternating and block polyanions more than differences in the nature of electrostatic correlations within the brush.

3.3 Equilibrium Polymer Conformations

In this section, we interpret the static conformations of polymers for both overcharged and undercharged cases by computing the density profiles of neutral and charged blocks of both polyanions and polycations.

3.3.1 Nearly Neutral Cases and Overcharged Cases ($N_{pa}/N_{pc} = 1.125$)

Figures 5(a)–(d) display the density profiles of all the polyelectrolyte moieties for different charge sequences at $N_{pa} = 72$ ($N_{pa}/N_{pc} = 1.125$). The density profile of the neutral spacer block is almost identical across all charge sequences. For cases wherein the polyanion has an alternating charge sequence, the density profile of the charged block of the polyanion is indistinguishable from that of the neutral block (Block-Alter and Alter-Alter) and hence only the density profile of the charged block of the polyanion is shown.

For the Block-Block case in Fig. 5(a), the density profile of the charged block of the polyanion closely follows that of the charged block of the polycation, showing that the charged blocks align with each other. Such an arrangement is a direct consequence of the minimization of the electrostatic potential. The density profile of the neutral block of the free polyanions shows that the majority of these blocks “stick out” of the brush into the solution, but also a fraction instead penetrate deeper into the brush region. Al-

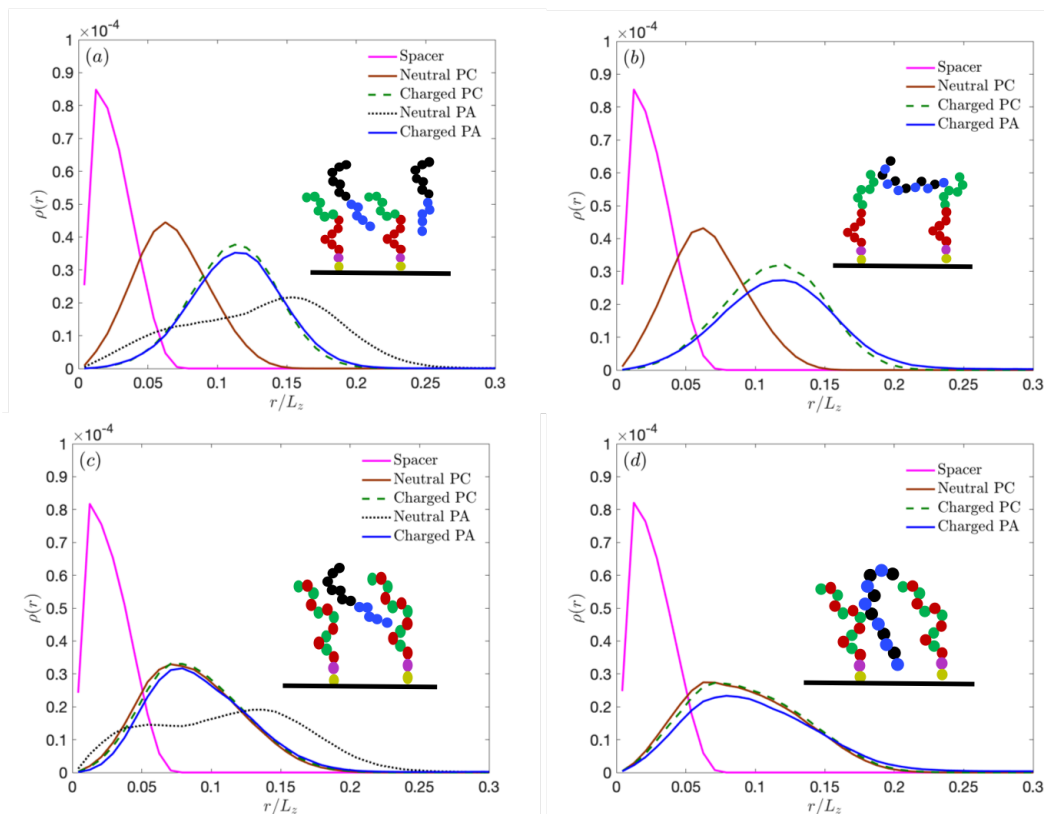


Fig. 5 Density distribution of spacer block of polycation (solid magenta), neutral block of polycation (solid brown), charged block of polycation (dotted green), neutral block of polyanion (dotted black), and charged block of polyanion (solid blue) as a function of distance from the grafted surface (normalized to the box length in the direction perpendicular to the graft plane) for (a) Block-Block; (b) Block-Alter; (c) Alter-Block and; (d) Alter-Alter charge sequences and $N_{pa} = 72$. For cases wherein the charged block of the polyanion is indistinguishable from the neutral block of the polyanion, only the charged block of the polyanion is shown. The schematic inside each figure depicts a graphical summary of the plots. The color coding of the schematic follows that of the plot.

though neutral block of the diblock copolymer does not have a preferential alignment, due to the steric hindrance (loss of conformational entropy) within the brush region, they “stick out” of the brush region. The fact that the peak in the density profile of the neutral block of the polycation lies between that of the spacer block and the charged block of the polycation reflects the connectivity of the three blocks and shows that the tethered chains are extended somewhat away from the wall.

The resulting equilibrium configuration is graphically represented in the inset of Fig. 5(a). The snapshot of the charged moieties shown in Fig. S7 is consistent with the configuration described above.

For the Block-Alter case in Fig. 5(b), the density profile of the charged units of the alternating polyanion closely follow the density of the charged block of the polycation. The profile of the neutral units of the polyanion is not shown separately because it is indistinguishable from that of the charged units of the same chain. The density profiles of the three blocks of the tethered block polycation are similar to those found for the Block-Block case.

For the Alter-Block case (Fig. 5(c)), the density profiles of the neutral and charged units within the polycation are very similar to each other, and to the density of the charged block of the polyanion. The profile of charged units of the polycation is spread

out over a larger range of values of z when the polycation is alternating than when it is tethered, which also forces the polyanion to penetrate deeper into the brush to compensate the polycation charge. The neutral block of the polyanion tends to preferentially “sticks out” of the brush, similar to the Block-Block case.

For the Alter-Alter case (Fig. 5(d)), the density profiles of the four blocks (neutral blocks of polyanion and polycation, charged blocks of polyanion and polycation) are almost identical to each other. As in the other cases, the profiles of the oppositely charged blocks align to produce approximate local charge neutrality, while neutral units of alternating chains are forced to follow charged units by the connectivity of the chains.

3.3.2 Undercharged Cases ($N_{pa}/N_{pc} = 0.5$)

Figure 6 displays the density profile of different blocks of the polyanion and polycation chains for $N_{pa} = 32$ ($N_{pa}/N_{pc} = 0.5$). The density profiles of the spacer blocks remain similar to that of the overcharged case above (Fig. 5) and hence are not shown in the Fig. 6. The density profile of the neutral block of the polycation in the Block-Block case is almost identical to that of the Block-Block case in the overcharged situation (Fig. 5(a)). The neutral block of the polyanion (dotted black) for the undercharged case sticks out of the brush. Similar arguments presented for the overcharged cases in the previous section, based on steric

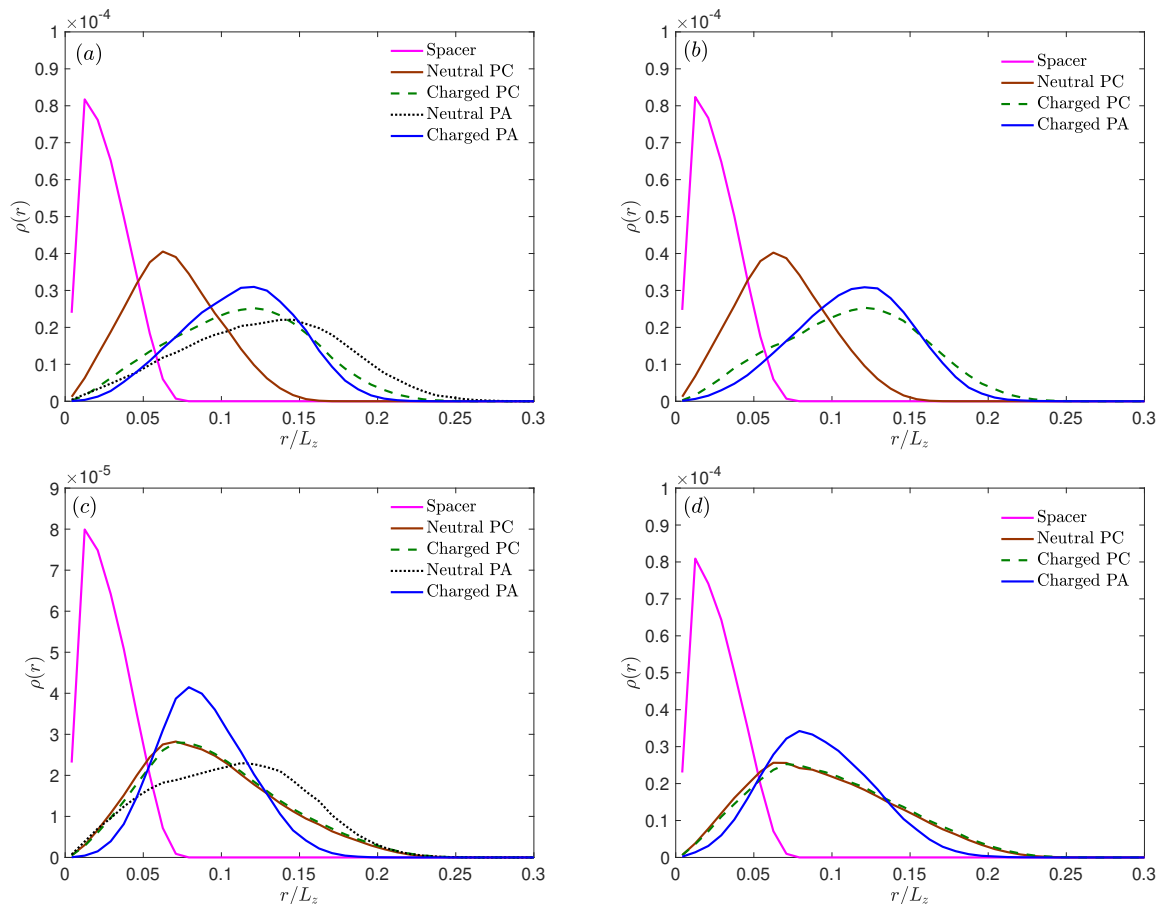


Fig. 6 Density distribution of neutral block of polycation (solid brown), charged block of polycation (dotted green), neutral block of polyanion (dotted black), and charged block of polyanion (solid blue) as a function of distance from the grafted surface (normalized to the box length in the direction perpendicular to the graft plane) for (a) Block-Block; (b) Block-Alter; (c) Alter-Block and; (d) Alter-Alter charge sequences and $N_{pa} = 32$. For cases wherein the charged block of the polyanion is indistinguishable from the neutral block of the polyanion, only the charged block of the polyanion is shown.

hindrances, can be used to rationalize this result.

Nevertheless, the density profile of the charged blocks of the polyanion do not follow that of the polycations as in the case of overcharged situations. To rationalize this result we compare the extension of the brush into the bulk, by comparing the value of the abscissa (z/L_z) at which the concentration of the polycation decays to 95% of its maximum value, between the overcharged and the undercharged cases. The brush extends more into the solution for the undercharged case ($z/L_z \approx 0.22$) compared to that for the overcharged case ($z/L_z \approx 0.18$) in Fig. 5(a) which results in a larger space for the polyanions within the brush region for the undercharged case. Further, for undercharged cases, counterion release occurs to maximize the entropy of the system, leading to a larger void volume within the brush region for the polyanions to explore. Together, the polyanion finds more space to reorient compactly within the brush region to maximize their conformational entropy, and to minimize their enthalpic penalties.

For all the other undercharged cases, *i.e.*, Block-Alter (Fig. 6(b)), Alter-Block (Fig. 6(c)), and Alter-Alter (Fig. 6(d)), the density profiles of the charged block of the polyanion chains follow closely that of the neutral block due to monomer connectivity. Nevertheless, unlike their overcharged counterparts,

the density profiles of the polyanion (neutral and charged) differ significantly from that of the charged block of the polyanion. To rationalize this, we again note that the brush is extended in the undercharged cases leading to a compact reorientation of the polyanion chains within the brush.

3.4 Charge Distribution in Brush and Bulk Regions

From the previous discussion, it is clear that the adsorption efficacy is maximum for the Block-Block case and weakest for the Alter-Alter case. However, the question remains as to whether there is any influence of charge sequence in the distribution of charges within the system. To this end, we compute the charge density profiles $q(z)$ as a function of the distance normal to the grafted surface z , and the total charge within the brush region Q_b for different charge sequences.

Figure 7(a) displays the smoothed charge densities (original density profiles are displayed in Fig. S8(a)) as a function of distance from the grafted surface for high polyanion concentrations, $N_{pa} = 100$ ($N_{pa}/N_{pc} = 1.5625$). The charge densities at this concentration show considerable variations with respect to changes in the charge sequence in the polyelectrolytes. For the concentration shown in Fig. 7(a), significant overcharging and

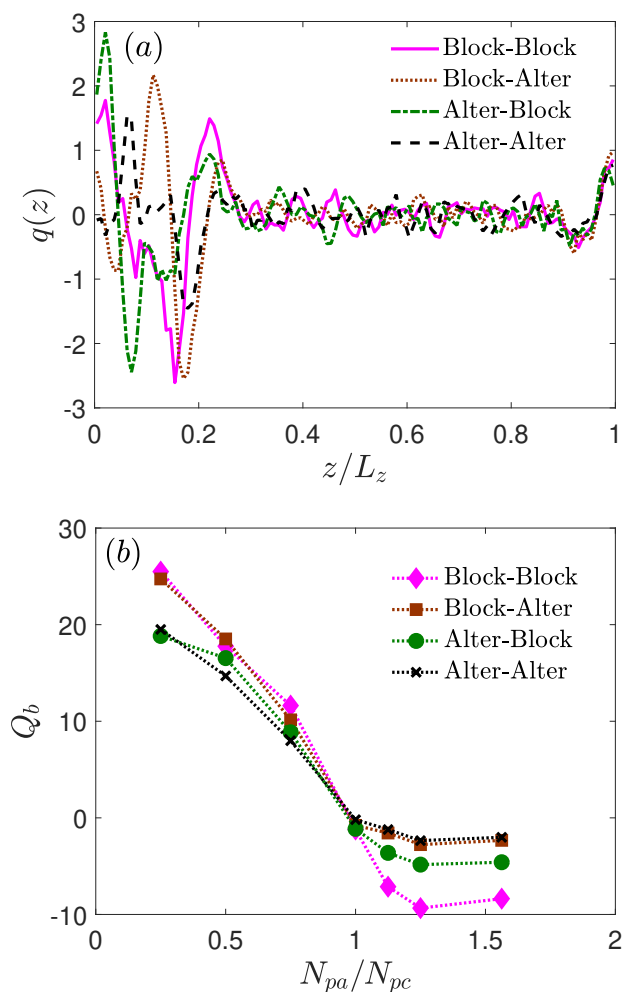


Fig. 7 (a) Smoothed charge distribution as a function of distance from the grafted surface, z , for $N_{pa} = 100$; (b) Net charge within the brush region as a function of the ratio between the number of polyanions to polycations N_{pa}/N_{pc} . We do not estimate error bars for this plot.

release of counterions are expected. For the Block-Block case, the charge density is dominantly positive near the grafted surface ($z/L_z < 0.1$), whereas the charge density near the edge of the brush ($z/L_z \approx 0.17$) is dominantly negative. These results suggest that the block polyanions align near the brush edge, consistent with the density profiles of polyelectrolytes presented in Sec. 3.2. In contrast, the peaks for the Alter-Alter case are not as pronounced as those of the other charge sequences, indicating that the polyanions are distributed more uniformly within the brush, and are again consistent with the results discussed in Sec. 3.2.

A drop in the values of charge densities is observed near the non-grafted side of the box at high polyanion concentrations. This dip is an artifact of the potential U_{wall} . The polyanions tend to be pushed further away from the wall than the small ions, leading to a small amount of charge separation. The upper wall is sufficiently far from the brush that the artifact arising at the upper wall is screened by the bulk of the solution, and thus has no impact on the charge within the brush. Spatial charge density profiles at low polyanion concentrations show lesser variations between different charge sequences (Fig. S8(b)).

To understand the effect of overcharging within the brush, Fig. 7(b) displays the net charge in the brush region for different polyanion to polycation chain ratios. At low concentration of the polyanion chains, the net charge within the brush is positive, which shows that no overcharging of the brush is observed. In contrast, when the number of polyanion chains are in excess of that of the polycation chains, overcharging of the brush is observed. These results are intuitive and are consistent with the literature.^{43,44} Overcharging of the brush is found to be strongest when both the polyanion and polycation possess block architecture and the weakest when both the polycation brush and the bulk polyanions possess an alternating architecture. This is consistent with Fig. 2(a), wherein the fraction of polyanions adsorbed is maximum for the Block-Block case.

4 Conclusions

In this work, we investigated the influence of charge sequence of polyelectrolytes upon their adsorption into oppositely charged polyelectrolyte brushes. We have considered situations in which either the free chains or tethered chains are in excess. In both situations, differences in the strength of adsorption among different choices of charge sequences arise primarily from differences in the change of energy upon adsorption, rather than differences in the change of entropy.

When the number of free chains in the simulation is less than the number of the tethered chains, all the free chains adsorb into the brush. The free energy of binding is found to be strongest when both the free and tethered chains have a block charge sequence and weakest when they both have an alternating charge sequence. Systems with one block copolymer and one alternating copolymer (Block-Alter or Alter-Block) have adsorption efficacies that lie between these extreme cases. For these two mixed cases, the system in which the free chain is a block copolymer exhibits a larger binding free energy. When the number of adsorbed chains is much less than the number of tethered chains, the free energy decrease upon adsorption is dominated by an increase in entropy. We assume that, in this limit, this entropy change arises primarily from counterion release. As the number of adsorbed chains approaches the number of tethered chains, the measured entropic driving force steadily decreases and the decrease in energy upon adsorption plays a more important role in driving adsorption.

When $N_{pa}/N_{pc} > 1$, overcharging of brushes is observed. Overcharging is strongest when both free and brush chains have a block charge sequence and weakest when both the free and brush chains have alternating sequences. Adsorption is somewhat stronger when the free chain has a block sequence and the tethered chain is alternating than the reverse.

Acknowledgements

The authors acknowledge fruitful discussions with Boris Shklovskii at the School of Physics and Astronomy, University of Minnesota. This work was supported primarily by the National Science Foundation through the University of Minnesota Materials Science Research and Engineering Center under Award No. DMR-1420013. The authors acknowledge the Minnesota Supercomputing Institute (MSI) at the University of Minnesota for pro-

viding resources that contributed to the research results reported within this paper.

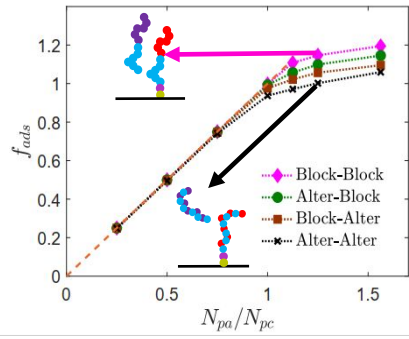
Code Repository

LAMMPS and analysis codes used in this article are available at https://github.com/vaidyanathanms/polyelectrolyte_sequencedependence.git.

Notes and references

- 1 C. W. Pak, M. Kosno, A. S. Holehouse, S. B. Padrick, A. Mittal, R. Ali, A. A. Yunus, D. R. Liu, R. V. Pappu and M. K. Rosen, *Mol. Cell*, 2016, **63**, 72 – 85.
- 2 J. W. Hong, W. L. Hemme, G. E. Keller, M. T. Rinke and G. C. Bazan, *Adv. Mater.*, 2006, **18**, 878–882.
- 3 A. Kabanov and V. Kabanov, *Adv. Drug Delivery Rev.*, 1998, **30**, 49–60.
- 4 M. Balastre, F. Li, P. Schorr, J. Yang, J. W. Mays and M. V. Tirrell, *Macromolecules*, 2002, **35**, 9480–9486.
- 5 G. Decher, *Science*, 1997, **277**, 1232–1237.
- 6 Y.-H. Lin and H. S. Chan, *Biophys. J.*, 2017, **112**, 2043 – 2046.
- 7 E. Kizilay, A. B. Kayitmazer and P. L. Dubin, *Adv. Colloid Interface Sci.*, 2011, **167**, 24 – 37.
- 8 S. M. Louie, R. D. Tilton and G. V. Lowry, *Environ. Sci. Technol.*, 2013, **47**, 4245–4254.
- 9 D. Priftis and M. Tirrell, *Soft Matter*, 2012, **8**, 9396–9405.
- 10 Y. Yeo, E. Bellas, W. Firestone, R. Langer and D. S. Kohane, *J. Agric. Food. Chem.*, 2005, **53**, 7518–7525.
- 11 S. Lankalapalli and V. R. M. Kolapalli, *Indian J. Pharm. Sci.*, 2009, **71**, 481–487.
- 12 Z. Liu, Y. Jiao, Y. Wang, C. Zhou and Z. Zhang, *Adv. Drug Delivery Rev.*, 2008, **60**, 1650 – 1662.
- 13 C. Cooper, P. Dubin, A. Kayitmazer and S. Turksen, *Curr. Opin. Colloid Interface Sci.*, 2005, **10**, 52 – 78.
- 14 D. Sprouse and T. M. Reineke, *Biomacromolecules*, 2014, **15**, 2616–2628.
- 15 P. T. Hammond, *Adv. Mater.*, 2004, **16**, 1271–1293.
- 16 J. D. Mendelsohn, C. J. Barrett, V. V. Chan, A. J. Pal, A. M. Mayes and M. F. Rubner, *Langmuir*, 2000, **16**, 5017–5023.
- 17 H. Ai, S. A. Jones and Y. M. Lvov, *Cell Biochem. Biophys.*, 2003, **39**, 23.
- 18 B. Schoeler, G. Kumaraswamy and F. Caruso, *Macromolecules*, 2002, **35**, 889–897.
- 19 J. Borges and J. F. Mano, *Chem. Rev.*, 2014, **114**, 8883–8942.
- 20 P. A. Patel, J. Jeon, P. T. Mather and A. V. Dobrynin, *Langmuir*, 2005, **21**, 6113–6122.
- 21 L.-W. Chang, T. K. Lytle, M. Radhakrishna, J. J. Madinya, J. Vázquez, C. E. Sing and S. L. Perry, *Nat. Commun.*, 2017, **8**, 1273.
- 22 V. S. Rathee, H. Sidky, B. J. Sikora and J. K. Whitmer, *J. Am. Chem. Soc.*, 2018, **140**, 15319–15328.
- 23 J. T. G. Overbeek and M. J. Voorn, *J. Cell. Physiol.*, 1957, **49**, 7–26.
- 24 K. Shen and Z.-G. Wang, *J. Chem. Phys.*, 2017, **146**, 084901.
- 25 P. Zhang, N. M. Alsaifi, J. Wu and Z.-G. Wang, *Macromolecules*, 2016, **49**, 9720–9730.
- 26 M. Muthukumar, *J. Chem. Phys.*, 2004, **120**, 9343–9350.
- 27 M. Muthukumar, *Macromolecules*, 2017, **50**, 9528–9560.
- 28 K.-i. Tainaka, *J. Phys. Soc. Jpn.*, 1979, **46**, 1899–1906.
- 29 A. Kudlay and M. Olvera de la Cruz, *J. Chem. Phys.*, 2004, **120**, 404–412.
- 30 A. Kundagrami and M. Muthukumar, *J. Chem. Phys.*, 2008, **128**, 244901.
- 31 R. R. Netz and J.-F. Joanny, *Macromolecules*, 1999, **32**, 9013–9025.
- 32 R. R. Netz and J.-F. Joanny, *Macromolecules*, 1999, **32**, 9026–9040.
- 33 K.-i. Tainaka, *J. Phys. Soc. Jpn.*, 1983, **52**, 2603–2609.
- 34 B. Peng and M. Muthukumar, *J. Chem. Phys.*, 2015, **143**, 243133.
- 35 R. Kumar, D. Audus and G. H. Fredrickson, *J. Phys. Chem. B*, 2010, **114**, 9956–9976.
- 36 J. Lee, Y. O. Popov and G. H. Fredrickson, *J. Chem. Phys.*, 2008, **128**, 224908.
- 37 Y. O. Popov, J. Lee and G. H. Fredrickson, *J. Polym. Sci., Part B: Polym. Phys.*, 2007, **45**, 3223–3230.
- 38 V. Pryamitsyn and V. Ganesan, *Macromolecules*, 2014, **47**, 6095–6112.
- 39 J. Qin and J. J. de Pablo, *Macromolecules*, 2016, **49**, 8789–8800.
- 40 K. Shen and Z.-G. Wang, *Macromolecules*, 2018, **51**, 1706–1717.
- 41 S. L. Perry and C. E. Sing, *Macromolecules*, 2015, **48**, 5040–5053.
- 42 M. Radhakrishna, K. Basu, Y. Liu, R. Shamsi, S. L. Perry and C. E. Sing, *Macromolecules*, 2017, **50**, 3030–3037.
- 43 Q. Cao, C. Zuo and L. Li, *Phys. Chem. Chem. Phys.*, 2011, **13**, 9706–9715.
- 44 Z. Ou and M. Muthukumar, *J. Chem. Phys.*, 2006, **124**, 154902.
- 45 D. J. Sandberg, J.-M. Y. Carrillo and A. V. Dobrynin, *Langmuir*, 2007, **23**, 12716–12728.
- 46 J. Yang, Z. Hua, T. Wang, B. Wu, G. Liu and G. Zhang, *Langmuir*, 2015, **31**, 6078–6084.
- 47 A. B. Kayitmazer, D. Seeman, B. B. Minsky, P. L. Dubin and Y. Xu, *Soft Matter*, 2013, **9**, 2553–2583.
- 48 S. Kim, J. Huang, Y. Lee, S. Dutta, H. Y. Yoo, Y. M. Jung, Y. Jho, H. Zeng and D. S. Hwang, *Proc. Natl. Acad. Sci. U.S.A.*, 2016, **113**, E847–E853.
- 49 T. T. Nguyen and B. I. Shklovskii, *Phys. Rev. Lett.*, 2002, **89**, 018101.
- 50 A. Y. Grosberg, T. T. Nguyen and B. I. Shklovskii, *Rev. Mod. Phys.*, 2002, **74**, 329–345.
- 51 R. Zhang and B. Shklovskii, *Phys. A*, 2005, **352**, 216 – 238.
- 52 H. William, D. Andrew and S. Klaus, *J. Mol. Graphics*, 1996, **14**, 33 – 38.
- 53 M. P. Allen and D. J. Tildesley, *Computer Simulation of Liquids*, Clarendon Press, New York, NY, USA, 1989.

- 54 G. Rajagopal and R. Needs, *J. Comput. Phys.*, 1994, **115**, 399 – 405.
- 55 B. A. Luty, M. E. Davis, I. G. Tironi and W. F. V. Gunsteren, *Mol. Simul.*, 1994, **14**, 11–20.
- 56 I.-C. Yeh and M. L. Berkowitz, *J. Chem. Phys.*, 1999, **111**, 3155–3162.
- 57 S. Plimpton, *J. Comput. Phys.*, 1995, **117**, 1 – 19.
- 58 B. Roux, *Comput. Phys. Commun.*, 1995, **91**, 275 – 282.
- 59 J. A. Lemkul and D. R. Bevan, *J. Phys. Chem. B*, 2010, **114**, 1652–1660.
- 60 S. Park, F. Khalili-Araghi, E. Tajkhorshid and K. Schulten, *J. Chem. Phys.*, 2003, **119**, 3559–3566.
- 61 S. Kumar, J. M. Rosenberg, D. Bouzida, R. H. Swendsen and P. A. Kollman, *J. Comput. Chem.*, 1992, **13**, 1011–1021.
- 62 A. Grossfield, *WHAM: the weighted histogram analysis method, version 2.0.9.1*.
- 63 G. Fiorin, M. L. Klein and J. Hénin, *Mol. Phys.*, 2013, **111**, 3345–3362.
- 64 A. M. Smith, A. A. Lee and S. Perkin, *J. Phys. Chem. Lett.*, 2016, **7**, 2157–2163.
- 65 A. Grossfield and D. M. Zuckerman, *Annu. Rep. Comput. Chem.*, 2009, **5**, 23 – 48.



The influence of backbone charge sequence in oppositely charged polyelectrolyte brushes upon their adsorption efficacy is reported at low salt concentration using coarse-grained molecular dynamics simulations.